Investigation of Bubble Penetration Through Interface Between Immiscible Liquids

Check for updates

Xiangfeng Cheng, Baojun Zhao, Fuming Zhang, Gele Qing, and Zhixing Zhao

Abstract As an important source of copper losses to the slag, SO_2 bubbles formed in the quiescent settlement zone of smelting furnace bring matte into slag phase through the immiscible matte-slag interface. The penetration and entrainment mechanisms of large bubbles were studied while the entrainment by micro bubbles was rarely investigated. In this paper, attachment of matte droplets to micro SO_2 bubbles in the industrial smelting slags and laboratory samples have been confirmed by high-temperature experiments. The bubble penetration behaviors through liquid–liquid interface were simulated by the cold model experiments using water and silicone oil. Results showed that fine gas bubbles can pass through the liquid–liquid interface and cause the heavier liquid entrainment. Although the critical bubble penetration size deduced in previous studies is inconsistent with the phenomenon observed in cold model experiments, it is an important parameter to classify the bubble entrainment regimes which is closely associated with the bubble penetration regimes. Greene's theoretical derived values of critical bubble penetration and entrainment sizes are in good agreement but comparatively higher than the experimental results. The Weber numbers based on the critical bubble penetration size, heavier liquid density, and interfacial tension under different experimental conditions are normally between 4 and 4.5.

Keywords Copper loss · Micro bubbles · Liquid–liquid interface · Penetration mechanisms

X. Cheng (✉) · G. Qing · Z. Zhao
Shougang Research Institute of Technology, Beijing 100043, China
e-mail: xiangfeng_2008@126.com

B. Zhao
International Research Institute for Resources, Energy, Environment and Materials, Jiangxi University of Science and Technology, Jiangxi 341099, China
e-mail: bzhao@jxust.edu.cn

F. Zhang
Shougang Group, Beijing 100041, China
e-mail: zhangfuming2018@163.com

Introduction

The bottom blowing smelting furnace (BBF) and Teniente Converter (TC) are the two important bath copper smelting furnaces used mainly in China and Chile, respectively. BBF injects high pressures gases (high oxygen enrichments: approximately 70%) into the bath using 7° and 22° oxygen lances and is operated at l160–1200 °C [1]. The gases with low oxygen enrichments (35–42%) were applied in TC and injected horizontally at relatively low pressures [2], and the operating temperature of TC is around 1250 °C. The average copper content in BBF slag is around 3.5 wt%, while the copper content in TC smelting slag is controlled to be around 9 wt%.

In the smelting process, copper concentrate would experience fierce oxidization with oxygen enriched air in the reaction zone, and then two stratified liquid layers would be formed in the relatively quiescent settlement zone. Theoretically, the slag phase (approximately 0.5 m thick) above matte would be discharged cleanly through discharging hole at the end of the smelting furnace. However, the insufficient oxidization of copper concentrate in reaction zone would cause further oxidisation in the settlement zone, leading to numerous microbubbles generation in the matte phase, as shown in Eq. 1.

$$CuFeS_2(s) + O_2(g) + SiO_2(s)(Cu - Fe - S)(l)$$
$$+ FeO - SiO_2(l) + SO_2(g) + heat \tag{1}$$
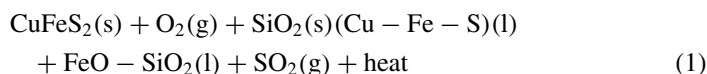
Several experimental and numerical studies were carried out on bubble passage through the immiscible liquid–liquid interface by cold model experiments. Some researchers proposed that there exists a critical bubble size that could provide sufficient upward force to overcome the interfacial tension to pass through the interface between superposed liquid layers, and the criterion for the size evaluation depends on liquids surface tensions and densities [1–3]. However, some studies reported that the bubble would be trapped at the interface for milliseconds to minutes if the bubble buoyancy force and inertia force cannot overcome interfacial tension. With the drainage of disjoining film between bubble and interface, the bubble would eventually pass through the interface when the film reaches a critical thickness, which contradicts previous theories [4–6]. Considering the precondition of heavier liquid entrainment by rising gas bubbles is that those bubbles are capable of penetrating the liquid–liquid interface; it is necessary to carry out further studies on fine bubble penetration behaviors and their corresponding entrainment regimes. Meanwhile, quite limited research attached importance to the metal entrainment by bubbles in molten metal-slag systems at high-temperature specifically until now. Therefore, the present study was to clarify the fine bubble penetration behaviors at a liquid–liquid interface in cold model experiments by integrating the analysis of as-received industrial slag samples.

In this work, the industrial slag samples from the bottom-blown furnace (BBF) and side-blown furnace (TC) were analysed by Scanning Electron Microscope (SEM)

to evaluate the SO_2 bubble effects on matte entrainment. Flow regimes of fine and large bubbles at the liquid–liquid interface were observed by high-speed camera, and the suitable equations suitable to predict bubble terminal velocities were compared. Critical bubble sizes to classify the flow regimes were compared.
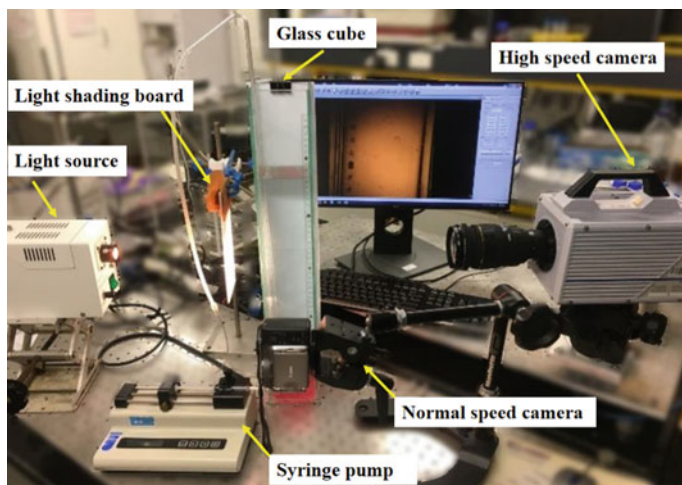
Experimental

Materials

Liquid–liquid systems in cold model experiments were designed with varying chemical compositions, namely silicone oils (10cP, 50cP, 100cP, 200cP, 500cP, Sigma-Aldrich, USA), SDS (Sodium Dodecyl Sulphate) (99.0%, Sigma-Aldrich, USA), Glycerol (99.0%, Sigma-Aldrich, USA), and $CaCl_2$ (93.0%, Sigma-Aldrich, USA). SDS powder was added into the solution to adjust surface tension without density and viscosity variation. Glycerol solutions of different weight percentages (80, 70, 60, and 40%) were used to change heavier liquid viscosities, and the liquid viscosity could increase from 60 to 3.72cP, while the density and surface tension remained constant by adding SDS powder. The Calcium Chloride of different weight percentages was used to change heavier liquid density due to the high solubility in water. Interfacial tension was determined as the difference between the surface tension of the two liquids. Water, glycerol, $CaCl_2$, and silicone oils were used to create a series of liquid–liquid interface systems. The liquid combinations were chosen to cover a broad range of interfacial tensions, viscosities, and density ratios, as shown in Table 1.

Experimental Apparatus

The system consisted of a transparent glass container (80 mm × 80 mm × 600 mm), in which a single bubble was generated through a glass inlet tube connecting with a syringe pushed by a syringe pump. A high-speed camera was placed at the level of interface between immiscible liquids in front of the glass cube to capture the bubble penetration behaviours at 500 fps; a normal camera was used to make up the high-speed imaging defect of the limited view field. A light source (XGY-II) in the opposite direction of the high-speed camera was used to provide dispersed light through a light shading board to illuminate liquids in the glass cube. Air was injected from a syringe pushed by a syringe pump, and the flow rate was controlled using this syringe pump. The bubble size could be controlled through some specially-made glass nozzles which are replaceable in the notch of the gas injection tube. The experimental apparatus was shown in Fig. 1.

Table 1 Physical properties of liquid–liquid combination systems

Lower phase				Upper phase			
Material	Viscosity/cP	Density/(kg m^{-3})	Surface tension/(mN m^{-1})	Material	Viscosity/cP	Density/(kg m^{-3})	Surface tension/(mN m^{-1})
Glycerol (80%)	60.1	1210	48.06	Silicone oil	10	930	20.1
Glycerol (70%)	22.5	1190	48.26	Silicone oil	50	959	20.7
Glycerol (60%)	10.8	1160	48.11	Silicone oil	100	965	20.9
Glycerol (40%)	3.72	1100	48.66	Silicone oil	200	970	21.1
CaCl$_2$ (40%)	8.48	1420	58.03	Silicone oil	500	970	21.1
CaCl$_2$ (30%)	3.33	1300	58.28				
CaCl$_2$ (20%)	1.81	1190	57.00				

Fig. 1 Cold model experimental apparatus

Four bubble shapes were observed in cold model experiments, i.e. spherical, oblate ellipsoidal, oblate ellipsoidal cap, and spherical cap. Small bubbles tend to present a spherical shape and become elliptical when bubble size grows larger. The bubble size and terminal velocity were processed by ImageJ. Due to the deformation of rising bubbles, the equivalent bubble diameter was defined as

$$d_{eq} = \left(d_h^2 d_v\right)^{1/3} \tag{2}$$

where d_h and d_v are horizontal and vertical diameters, respectively.

Results and Discussion

Analysis of Industrial Slag Samples

A series of slag samples were collected during slag tappings in commercial BBF and TC and analysed by SEM systematically. The typical microstructures of the BBF and TC slag are shown in Fig. 2a, b, respectively. Quantitative analyses of 368 SEM images of industrial BBF and TC slags show that 14.8% and 11.2% matte droplets are attached to gas bubbles, respectively, compared to 0.2% and 0.4% matte droplets attached to spinel solids. The average bubble size in BBF and TC slags is 130 µm and 168 µm, respectively, with a maximum bubble size of 1800 µm. The attachment between matte and micron bubbles in the industrial slag samples demonstrates the
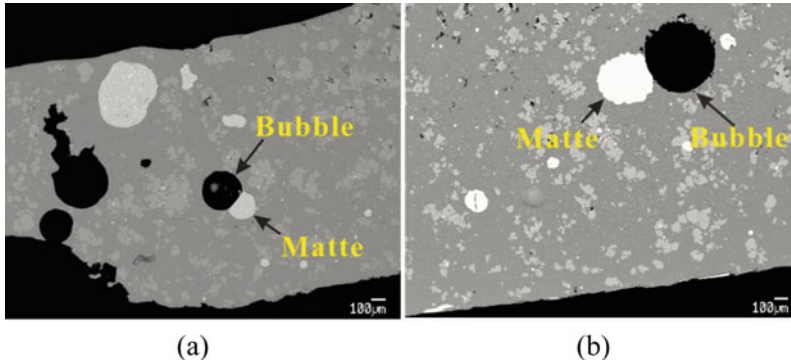
Fig. 2 Attachment between matte droplets and SO$_2$ bubbles in BBF slags **a** and TC slags **b**

significant effect of micro bubbles on matte entrainment in the matte-slag system at the high temperature.

Small Bubble Penetration Behaviors

In cold model experiments, some small bubbles, usually smaller than 3 mm in diameter, cannot penetrate the interface directly and will dwell for a short period as reported in previous studies [1–3]. To visualize the small bubble penetration and entrainment behaviours at the interface, high-speed imaging techniques were used in cold model experiments.

The sequential photographs of the whole penetrating process of a small bubble (2.5 mm in diameter) through a water-10cP silicone oil interface were shown in Fig. 3. The interfacial force between water and silicone oil tends to prevent the bubble from crossing the interface and makes bubbles dwell at the interface for up to several seconds as shown in Fig. 3a. The thin bubble cap film will drain gradually from the bubble top surface due to the pressure gradient in this period. When bubble cap film is thin enough, the gas bubble will break up the interface and rise to the top at $t = 0.005$ s, as shown in Fig. 3b. The whole heavier liquid peeled off the gas bubble completely within 0.01 s and began to detach from the interface, as shown in Fig. 3c–e. No visible water column is formed in this process due to the insufficient buoyancy force for smaller gas bubbles to penetrate the interface directly and drag denser liquid globules into the upper phase. The formation of water columns behind gas bubbles is associated with the immiscible liquid properties and interfacial tension force [5]. The short denser liquid bridge connecting bubble and interface shown in Fig. 4e breaks eventually, and a small proportion remains stably at the bubble bottom surface. The whole duration time from bubble cap film rupture in Fig. 3a to complete detachment from an interface in Fig. 3f lasts only 0.067 s. It is hypothesized that the denser liquid entrainments by small gas bubbles are mainly in the form of thin
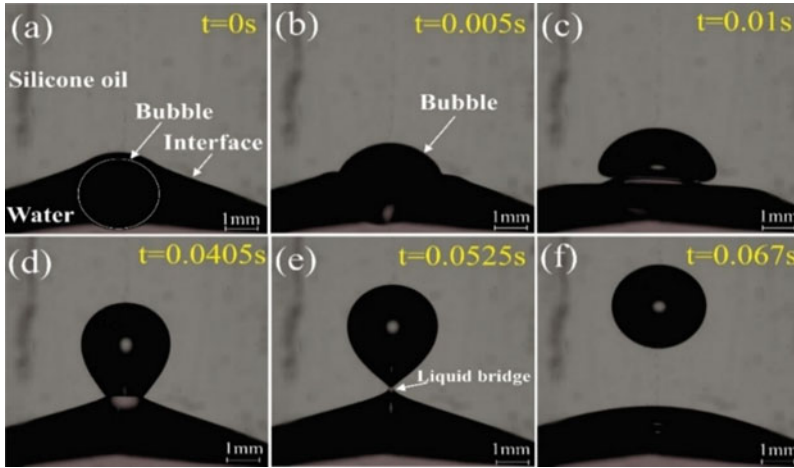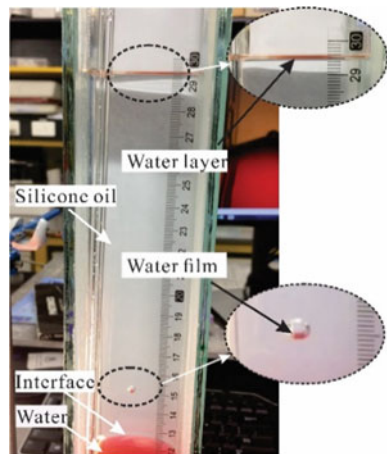
Fig. 3 Small gas bubble transporting behaviouor at interface

Fig. 4 Water layer
accumulation at silicone oil
surface after bubble rupture

liquid film accumulated at the bottom of rising bubbles. The surface tension of thin denser liquid film makes it difficult to peel off the bubble bottom surface to form a free denser liquid globule as shown in Fig. 3f. It should be noted that interfacial tension force counteracting bubble buoyancy force and inertia force at the first bubble impact would decrease with the drainage of bubble cap film due to the changing film thickness and interface curve, leading to the force unbalance [7, 8].

Although the thin water film is difficult to be identified directly from a series of photographs due to the limited film thickness and imaging technique limitation by high-speed camera, the water entrainment by a small-sized bubble was confirmed by a normal speed camera. Several gas bubbles with diameters controlled between 0.5 and 3 mm in cold model experiments were observed as shown in Fig. 4. The water

phase is dyed with red ink to provide good contrast between the enveloping water layer and the upper liquid. All fine bubbles passed through the interface eventually despite a short dwelling at the interface, and a thin red water film was found to be floating at the bottom of the rising bubble due to gravity force in front of the white background. With the accumulation of water droplets from the ruptured bubbles at the surface of the silicon oil, a clear thin red water layer was observed at the top of silicon oil as seen in Fig. 4. The observation in cold model experiments was consistent with the SEM analysis of industrial slags samples in Fig. 2, which shows a large number of matte droplets attachment to SO_2 gas bubbles (diameter: 0.016 –1.8 mm) in slag samples.

Medium Bubble Penetration Behaviours

Sequential photographs in Fig. 5a–f illustrate the penetration process of a medium gas bubble (5 mm in diameter) through a water-silicone oil 50 cP interface. The water column forms when a gas bubble attempts to penetrate the water-silicone oil interface at $t = 0.218$ s (Fig. 5b), and a discernible water layer covers the bubble surface at $t = 0.236$ s (Fig. 5c). After the water column breaks at a certain height, the water layer centres beneath the gas bubble due to the higher specific gravity (Fig. 5c). The water layer starts to peel off the gas bubble and forms a spherical water droplet underneath (Fig. 5d, e) which will detach from the bubble when interfacial tension can no longer support the gravity of the water droplet. The water droplet continues to rise due to the bubble wake effect and its original momentum (Fig. 5f) and settles after reaching
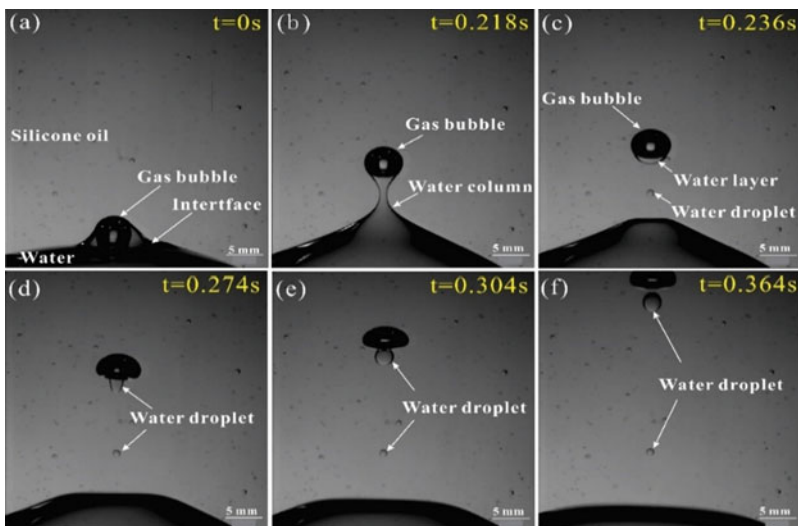
Fig. 5 Medium bubble penetrating behaviour at interface

a certain height in the silicon oil. Previous studies mainly focused on the heavier liquid entrainment by bubbles that can cross the interface directly and carry visible large liquid droplets into the upper phase and ignored the micro bubbles effect in the liquid–liquid system, particularly in metal-slag systems at high temperature [4–6, 9–11].
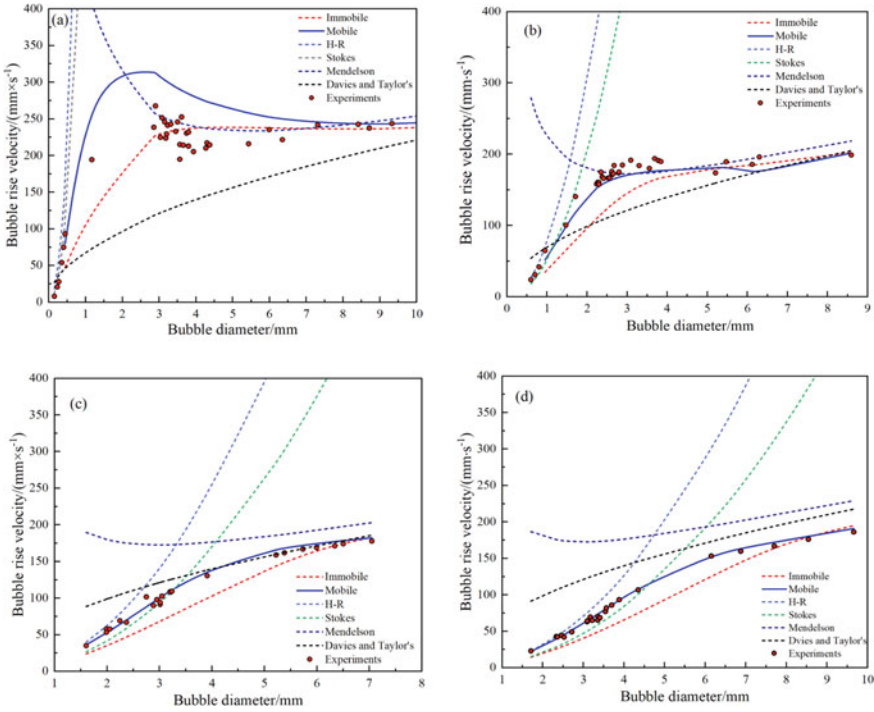
Bubble Terminal Rising Velocity

As a function of bubble rising velocity, Weber number *We* is an important dimensionless number and parameter in fluid mechanics to analyse an interface between two different fluids, particularly for multiphase flows with strongly curved surfaces. Bubble rising velocity is a complicated function of the bubble geometry, the liquid physical properties, and the physicochemical properties of the gas–liquid interface. A variety of equations were discussed to predict bubble rising velocity in different experimental conditions. The bubble penetration behaviours are essentially the result of the interaction of bubble buoyancy force, bubble inertia force, and interfacial tension force. Weber number *We* relating the inertia forces to the forces resulting from surface tension is indicative of the kinetic energy required to induce the interface deformation necessary for bubble passage, which is related to bubble rising velocity [4, 12]. Therefore, Stokes equation, Hadamard and Rybczynski equation (H-R), Mendelson equation, Davies and Taylor equation, and equation deduced by Travis to predict the rising velocities of bubbles based on previous studies were briefly discussed here [4, 13–15]. A high-speed camera was used to measure the bubble terminal velocity in water, 10 cP silicone oil, 50 cP silicone oil, and 100 cP silicone oil in cold model experiments as shown in Fig. 6a-d, respectively.

As we can see in Fig. 6a–d, Stokes or H-R equations can predict terminal velocity well for small bubbles in micron scale in different silicone oils. However, with the increase of bubble size, the terminal velocity correlation for bubble mobile surface conditions by Travis can well fit the experimental results with bubble size between 1 and 10 mm. Thus, it can be used to predict bubble velocity in cold model experiments considering a similar bubble size range. The terminal velocity correlation for bubble immobile surface conditions can predict bubble terminal velocity more precisely in pure water. Davies and Taylor's correlation and Mendelson's correlation are suitable for bubbles larger than 10 mm in diameter.

Discussion on Weber Number and Critical Bubble Penetration Size

Bubble penetration behaviours through the liquid–liquid interface are essentially the interaction result of bubble buoyancy force, inertial force, and interfacial tension.

Fig. 6 Comparison of correaltions to predict bubble terminal velocity

As a measure of the relative importance of the fluid's inertia compared to its surface tension, *We* can be used to characterize the kinetic energy of a rising bubble and the interfacial free energy from the interface to counteract this energy, as shown in Eq. 3.

$$We = \left(\frac{8}{C_D}\right)\frac{\left(\frac{\rho v^2}{2}C_D\pi\frac{d^2}{4}\right)}{(\pi d\sigma_I)} = \frac{\rho_2 v^2 d}{\sigma_I} \tag{3}$$

where v is bubble rising velocity, m/s; C_D is the drag coefficient; ρ_2 is the density of heavier liquid, kg/m^3; d is bubble diameter, m; σ_I is interfacial tension, N/m.

As shown in Fig. 3, fine bubbles dwelling at the interface due to the lower bubble buoyancy force and inertia force than interfacial tension can penetrate interface with the drainage of bubble cap film. However, whether bubbles can overcome interfacial tension and cross interface directly at the first impact has a significant influence on heavier liquid entrainment regimes by comparison between Figs. 3 and 4. It should be noted that the volume of visible heavier liquid layer suspending at the bottom of larger bubbles in Fig. 4 is much larger than the indiscernible liquid film enveloping the bubble surface. Thus, previous studies on critical bubble penetration and entrainment sizes make sense in classifying the heavier liquid entrainment methods by

rising bubbles. Greene et al. proposed the theoretical critical bubble penetration and entrainment volumes by balancing a static bubble buoyancy force and interfacial tension and compared with experimental results in cold model experiments [1, 2]. Furthermore, dimensionless number *We* using bottom liquid density and interfacial tension bubbles was analysed in experiments. Different from previous studies based on the static model, *We* can be used to measure the bubble penetration ability to cross interface at the first impact at the interface in dynamic conditions by considering inertia force. In other words, a high *We* number means higher kinetic energy to overcome the constant interfacial energy and could penetrate the interface directly.

As shown in Fig. 7a–d, the critical bubble penetration and entrainment sizes based on Greene's theory are very close but larger than experimental results in different experimental conditions, which is probably because Greene's model was built in static conditions and neglected bubble inertia force. With increasing the interfacial tension, the critical bubble penetration and entrainment size increase, which is in agreement with experimental results. The heavier liquid density has significant effects on bubble entrainment size but a slight influence on bubble penetration size, which also can be confirmed by experimental results. Upper and heavier liquid viscosity have little effect on those two critical bubble sizes, which can be seen from the tiny change of experimental data. It should be noted that the Weber number using
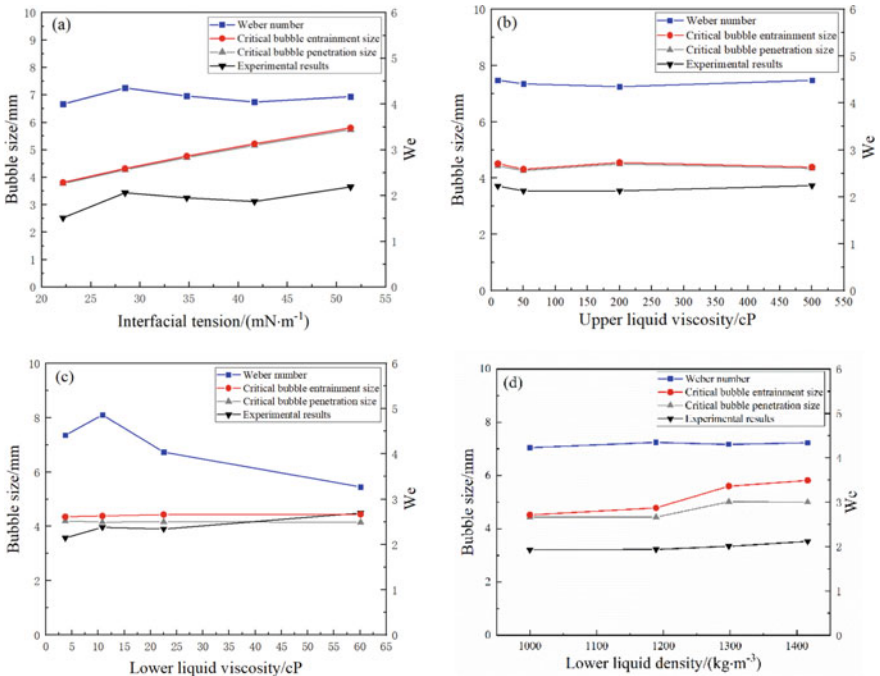
Fig. 7 Comparison of critical bubble size between Greene's theory experimental result and Weber number

bottom liquid density, interfacial tension, and critical bubble penetration size fluctuates around 4.25 between 4 and 4.5 under different experimental conditions, which is of great reference value to determine the heavier liquid entrainment regimes by small bubbles.

Conclusions

In this study, the attachment between micro bubbles and matte droplets in industrial slag samples was confirmed by SEM analysis. In cold model simulation experiments, small bubbles and larger bubbles penetration behaviours through immiscible liquids interface by the high-speed camera were investigated. It was found that fine bubbles stuck at the interface due to interfacial tension managed to cross interface with bubble cap film drainage, and thin indiscernible film enveloping bubbles was observed. Bubbles capable of penetrating interface directly tend to drag a liquid layer at the bottom surface stably, which could lead to heavier liquid entrainment in the upper phase. Greene's hypothesis about critical bubble penetration and entrainment sizes is basically in agreement with experimental results while a little higher. Weber number using bottom liquid density, interfacial tension, and critical bubble penetration size varied between 4 and 4.5, which could provide valuable guidance for industrial operations.

References

1. Greene GA, Chen JC, Conlin MT (1988) Onset of entrainment between immiscible liquid layers due to rising gas bubbles. Int J Heat Mass Transf 31(6):1309–1317
2. Greene GA, Chen JC, Conlin MT (1991) Bubble induced entrainment between stratified liquid layers. Int J Heat Mass Transf 34(1):149–157
3. Mori YH, Komotori K, Higeta K, Inada J (1977) Rising behavior of air bubbles in superposed liquid layers. Can J Chem Eng 55(1):9–12
4. Emery TS, Raghupathi PA, Kandlikar SG (2018) Flow regimes and transition criteria during passage of bubbles through a liquid-liquid interface. Langmuir 34(23):6766–6776
5. Kemiha M, Olmos E, Fei W, Poncin S, Li HZ (2007) Passage of a gas bubble through a liquid-liquid interface. Ind Eng Chem Res 46(19):6099–6104
6. Singh KK, Bart HJ (2015) Passage of a single bubble through a liquid–liquid Interface. Ind Eng Chem Res 54(38):9478–9493
7. Nguyen AV, Schulze HJ, Stechemesser H, Zobel G (1997) Contact time during impact of a spherical particle against a plane gas-liquid interface: theory. Int J Miner Process 50(1):97–111
8. Nguyen AV, Schulze HJ, Stechemesser H, Zobel G (1997) Contact time during impact of a spherical particle against a plane gas-liquid interface: experiment. Int J Miner Process 150(1):113–125
9. Dietrich N, Poncin S, Pheulpin S, Li HZ (2008) Passage of a bubble through a liquid-liquid interface. AIChE J 54(3):594–600
10. Morsi BI, Basha OM (2015) Mass transfer in multiphase systems. In: Solecki M (ed) Mass transfer—advancement in process modelling. IntechOpen, London, pp 189–217

11. Tanno M, Liu J, Gao X, Kim SJ, UEDA S, Kitamura SY (2017) Influence of the physical properties of liquids and diameter of bubble on the formation of liquid column at the interface of two liquid phases by the rising bubble. Metall Mater Trans B 48(6):2913-2921
12. Rapp BE (2017) Chapter 9 - Fluids. In: Rapp BE (ed) Microfluidics: microfluidics: modelling, mechanics and mathematics 2017. Elsevier, Oxford, pp 243–263
13. Talaia M (2007) Terminal velocity of a bubble rise in a liquid. World Acad Sci Eng Technol 1(4):220–224
14. Parkinson L, Sedev R, Fornasiero D, Ralston J (2008) The terminal rise velocity of 10–100 μm diameter bubbles in water. J Colloid Interface Sci 322(1):168–172
15. Celata GP, D'Annibale F, Marco PD, Memoli G, Tomiyama A (2007) Measurements of rising velocity of a small bubble in a stagnant fluid in one- and two-component systems. Exp Therm Fluid Sci 31(6):609–623